Low-energy hydrogen-ion scattering from metal surfaces: Trajectory analysis and negative-ion formation

W. R. Koppers, B. Berenbak, D. Vlachos,* U. van Slooten,† and A. W. Kleyn‡
FOM-Institute for Atomic and Molecular Physics, Kruislaan 407, 1098 SJ Amsterdam, The Netherlands
(Received 4 August 1997; revised manuscript received 26 January 1998)

A comparative study on negative ion formation in the scattering of a proton beam from both a clean and one monolayer of barium-covered Ag(111) surface is presented. The angular and energy dependence of the backscattered negative hydrogen ions as a function of incoming and azimuthal angles has been determined for a beam energy of 750 eV. The backscattered negative particles emerge from the surface as well as from deeper layers of the crystal. The angular dependence of the outgoing particles shows a very rich structure, which is explained by shadowing and blocking of the incoming and outgoing particles. In addition, the angular dependence of the outgoing neutral particles is determined. The essential features appear the same, but distinct differences can be observed. These are due to changes in the probability for negative ion formation as a function of outgoing angle. The energy distributions of the outgoing particles suggest a large penetration depth along the crystal channels. We have performed classical trajectory calculations that simulate the angular distributions of the backscattered particles very well. These calculations also show considerable penetration of particles into the bulk of the crystal and complicated zigzag trajectories through the bulk before leaving the crystal. The (electronic) stopping inside the Ag solid is at least one or two orders of magnitude smaller (<0.3 eV/Å at $E=700$ eV) than the values found in the literature. Comparing the Ag(111) data and the data of Ag(111) covered by one monolayer barium, we conclude that the barium atoms occupy lattice positions of the crystal. The overlayer must contain vacancies to accommodate the large size mismatch between the barium atoms and those of the substrate. [S0163-1829(98)06719-8]

I. INTRODUCTION

The study of the interaction of low-energy ions with surfaces has received considerable attention from a multitude of disciplines within chemistry and physics.[1,2] In particular, the charge exchange mechanisms governing the interaction have been studied in great detail because of their technological relevance in catalysis and surface processing.[3,4] A fundamental understanding of ion/surface collisions is also important for analytical techniques that involve the detection of backscattered low-energy ions leaving the surface, such as low-energy ion scattering (LEIS) and secondary ion mass spectrometry, where it is important to know the ionization probabilities in order to draw conclusions.[2,5]

Another important area of research involving ion/surface collisions is fusion research and technology.[6] Here, a detailed knowledge of the neutralization and subsequent positive and negative ion formation in ion/surface collisions is important for a basic understanding of plasma/wall interactions, divertor physics, and negative ion sources.[7] Negative ion formation has received considerable attention; negative hydrogen ion yields up to 30% have been found for positive ions scattered off low work-function surfaces, such as Cs- or Ba-covered metal surfaces.[3] The study of penetration into the crystal lattice is also important for a better understanding of plasma/wall interactions and divertor physics.[8–11]

The mechanisms governing negative ion formation in the scattering of protons at low work-function surfaces have received considerable attention from the surface science community in recent years, experimentally as well as theoretically.[6,3,12–14] In those studies, emphasis was primarily put on determining the yields of negative ions and the charge exchange mechanisms. The differential conversion efficiency η has been determined for certain scattering conditions, where $\eta = I(H^-)/[I(H^-)+I(H^0)]$ and I the intensity for ions and neutrals measured with the same detection efficiency. To our knowledge, the scattering dynamics has not been studied in great detail for hydrogen ions with incident energies ranging from 100 eV to 1 keV, scattered from metal surfaces at incoming angles where considerable penetration is important. However, trajectory calculations have been carried out for hydrogen atoms scattered off single-crystal surfaces at glancing angles, where no penetration is observed and the particles are scattered in the specular direction.[15] Some studies have been performed involving penetration of hydrogen into the solid, although no trajectory analysis was performed in those investigations.[16,17]

In the case of scattering a beam of protons from a metal surface, the neutralization is assumed to occur along the incoming trajectory; before the positive ion collides with the surface it is neutralized into an excited state via resonant neutralization and subsequently Auger deexcited into the ground state. Effectively, neutral hydrogen atoms are scattered from the surface. Sufficiently close to the surface the affinity level, located at 0.7 eV below the vacuum level, shifts down due to the image force attraction and broadens because of the overlap of atomic and metallic wave functions, which allows negative ions to be formed in a resonant process. On the exiting trajectory, depopulation of the affinity levels occurs.

In recent years, the interest in negative ion formation from nonmetallic surfaces has increased.[18,19] In those studies, it was found that negative ion yields up to 70%, and even

100%, could be obtained for O and F scattering off alkali halide surfaces under certain conditions; i.e., highly energetic beams (>10 keV) incident at glancing angles. Also high yields of negative hydrogen ions have been found for low-energy ion scattering (<5 keV) from oxide surfaces.[20] The results from the oxide surfaces were interpreted in much the same way as scattering off the alkali halide surfaces; the surface is considered to be ionic and the hole that is created in the formation of the negative ion is localized and does not travel along with the negative ion. Recently, we observed large negative hydrogen ion yields in H^+ scattering from a graphite surface.[7]

Detailed trajectory analyses have been carried out for noble gas ions and alkali ions scattered off metal surfaces in the incident energy range between 10 eV and 1 keV.[21,2,4] The scattering dynamics of alkali ions from metal surfaces has been studied in great detail, both experimentally and with the help of classical trajectory calculations.[22,23,4] For those systems it was found that scattering occurs primarily with the outermost layer of the solid. Charge-transfer dynamics in these systems has also been studied in detail.[3,4] By correlating their experimental results and calculations, Cooper and co-workers found evidence for a trajectory-dependent charge-transfer event.[24]

Recently, a trajectory effect in negative hydrogen ion formation has been suggested in model calculations of hydrogen particles scattered from a stepped metal surface. The fraction of negative ions turned out to be highly dependent on the step density at the surface, and whether the steps were going up or down.[25] Those calculations model previously obtained experimental observations very well.[26]

Clearly, a careful analysis of the trajectories of scattered ions is important for a detailed understanding of ion-surface interactions; it is crucial for unraveling local effects and trajectory effects in neutralization and negative ion formation.[27,24] In this paper we discuss the trajectories of scattered negatively charged and neutral hydrogen atoms from incoming positive ions with energies around 700 eV on single-crystal metal surfaces. The interaction of the incident hydrogen particles and the crystal atoms is governed by a sequence of binary collisions in this incident energy range.[27,2] The collision kinematics and dynamics allows for elemental analysis and structure studies of the outermost layer of a solid. The experimental results are analyzed with the help of computer simulations, and explained by shadowing and blocking effects. Noble gas ions such as He and Ne are used in scattering experiments because of their high neutralization efficiencies if scattered from layers deeper than the topmost layer. Backscattered neutrals remain hidden from the detector. Hydrogen particles, however, have a much smaller shadow cone, which makes them more suited to use in the low incident energy regime for structure analysis. This was already recognized by MacDonald and co-workers in the scattering and detection of positive hydrogen ions.[28,16] However, in the present study we use an alternative approach by probing scattered negative hydrogen ions, which give the opportunity of obtaining structural information to several layers depth. To our knowledge, the present study is the first structure analysis using the detection of scattered negatively charged hydrogen ions.

In an earlier paper, we studied negative hydrogen ion formation in the scattering of a beam of protons from two monolayers of barium deposited onto Ag(111).[29] We found negative ion yields of about 20% for outgoing angles smaller than 60°; the negative ion fraction decreased for larger outgoing angles. In this study, all angles were defined with respect to the surface normal. A simple model, describing resonant charge transfer calculated by the nonperturbative coupled angular modes method, which also takes the parallel velocity effect into account,[30,29] described the measured negative ion fractions very well. Structure was observed in the angular distributions of the negative ions, which was assigned to scattering from second-layer atoms of the crystal.

In this paper, we present a detailed experimental study and classical trajectory calculations of the scattering of hydrogen particles from a clean Ag(111) surface and one covered with one monolayer of barium. The angular distributions of the backscattered negative ions reveal a peak structure, which suggests that considerable penetration into the solid occurs in the incident energy regime around 700 eV. With the help of classical trajectory calculations we assign the peaks to classes of trajectories. The simulated angular spectra are in good agreement with the measured spectra. Further, we comment on the energy losses the ions have suffered on both the clean and on one monolayer of barium-covered Ag(111) surfaces, and also on the final charge state of the scattered particles.

II. EXPERIMENT

A. Apparatus

The experimental setup is described in detail elsewhere.[29] Briefly, it consists of two UHV chambers. In one (base pressure of 4×10^{-11} mbar), the crystal can be cleaned and characterized by x-ray photoelectron spectroscopy (XPS), thermal desorption spectroscopy, and work-function measurements. The work-function measurements are done with a Kelvin probe. The crystal can be transferred under UHV to a two-axis goniometer in the second chamber (base pressure of 1×10^{-10} mbar). This goniometer allows rotation of the target around an axis parallel to the surface, to change the incoming angle θ_i (which is measured with respect to the surface normal) and rotation around the surface normal, to change the azimuthal angle ϕ. The total scattering angle θ is defined as $\theta=180°-(\theta_i+\theta_f)$, with θ_f the outgoing angle of the particles. On this chamber, a differentially pumped electron impact source (VG,AG 60) is mounted which produces the H^+ ions. The incident energies of the ions can be varied between 100 and 1250 eV. The ion beam is purified using a Wien filter. Typical currents at the crystal position between 1 and 2 nA are measured. The scattered positive and negative ions are detected with a 90° cylindrical electrostatic energy analyzer, which has an energy resolution of $\Delta E/E=0.08$. In the scattering plane, the detector can be rotated from 45° to 180° with respect to the incoming beam and out of plane detection from $-15°$ to 90° is possible. The angular resolution of the detector is around 0.5°. Adjacent to this detector, a fraction detector is mounted, with which the differential conversion efficiency η can be determined, where $\eta=I(H^-)/[I(H^-)+I(H^0)]$ and I is the energy integrated intensity of the ions or neutrals. Particles entering the detector are detected by a channeltron. However, prior to detection,

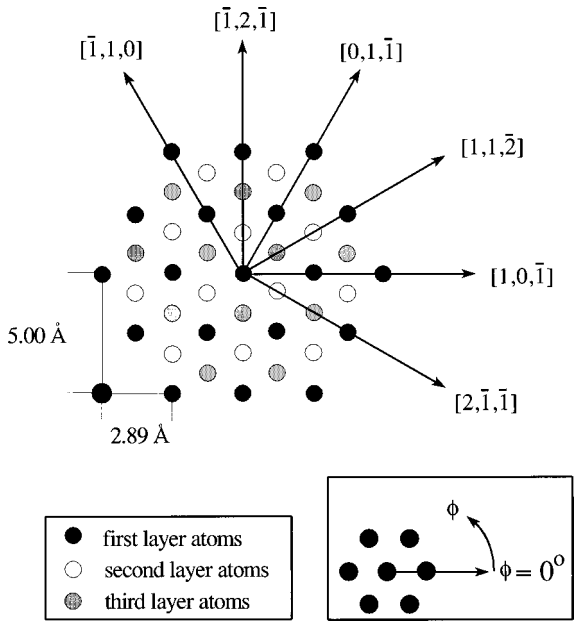

FIG. 1. Crystallographic drawing of the (111) face of a Ag crystal. The crystal directions and the definition of ϕ are indicated.

the ions are neutralized by reflection from a tungsten surface. In this way, a possible difference in detection efficiency for neutrals and ions is eliminated. When a retarding potential is applied at the entrance of the detector only the neutral particles are detected, if grounded, the total particle intensity is measured.

B. Crystal

The Ag(111) crystal is cut by spark erosion and polished mechanically. The misalignment of the (111) surface is less than 0.05° as determined by Von Laue diffraction. The crystal was cleaned by repeated sputter and anneal cycles. Typically, a sputter treatment consists of 15 min. of 800 eV Ar^+ bombardment at normal angle of incidence for a crystal current density of 5×10^{-6} A/cm^2. The crystal temperature during sputtering is 573 K. For annealing the crystal temperature is kept at 673 K for 15 min. The surface cleanliness is checked by XPS and work-function measurements. The crystal orientation is drawn in Fig. 1, in which the crystallographic directions are plotted. The (101) direction is defined as $\phi=0°$. All the spectra in this paper were measured with a crystal near room temperature. Good reproduction of earlier data[29] was found.

Onto the Ag(111) surface, barium is deposited from a SAES-Getter source. The pressure during dosing was below 2×10^{-10} mbar. The barium overlayer was previously characterized using Auger electron spectroscopy, XPS, work-function measurements, medium-energy ion scattering (MEIS), and low-energy H^+ scattering.[14,31,32] In the latter case, backscattered H^- ions were detected.[31] This work indicated that a monolayer of barium is initially grown, after which a rather open overlayer structure is formed by Poisson growth. It further showed that the overlayer grows epitaxially. Due to the difference in size of the adsorbate and substrate atoms, the first layer appears to be incomplete and must contain vacancies. The work function of a clean Ag(111) surface is 4.7 eV. When the surface is covered with one monolayer of barium the work function decreases to 2.4 eV.[14]

III. COMPUTATION

A. Potential

At incident energies that are high compared to the depth of the Ag-H potential well, only the repulsive part of the interaction potential is important for scattering. The repulsive Ag-H pair potential was calculated using the Hartree-Fock-Slater linear combination of atomic orbital method.[33] The results of this calculation are shown elsewhere.[34] The calculation can be approximated by a Born-Mayer potential which is of the form $V=A\exp(-\beta r)$.[33,23] The parameters are given by $A=3691.7$ eV and $\beta=7.134$ Å^{-1}.

B. Computer code

The computer code, written to simulate the scattering of the incoming particles at a crystal lattice, has been described extensively in the past[33,23] and is briefly summarized here. The code has been developed for collisions at (hyper)thermal energies and is rather inefficient in the present study compared to computer codes such as MARLOWE.[35,2] Nevertheless, satisfactory results are obtained.

Newton's equations are solved exactly for a hydrogen atom approaching a silver lattice, consisting of 321 atoms. The lattice is represented by five layers. In the first layer 88 atoms are placed, the second 74, the third 61, the fourth 54, and the fifth 44. The layers are placed on the Ag(111) lattice position sites. Thermal vibrations are taken into account using a so-called Einstein lattice.[23] These vibrations are generated using random displacements, according to the Boltzman distributions. The lattice is placed at $T=300$ K. The opening angle of the detector is set at 2°. The impact parameters are chosen systematically on a grid over the entire surface unit cell.

In a full three-dimensional calculation, a large number of hydrogen atoms are implanted into the crystal lattice or, otherwise, scattered out of the detection plane and hence are not detected. To obtain reasonable statistics, over 1×10^6 trajectories must be calculated. To gain more insight in the scattering dynamics and to reduce the number of trajectories, we performed calculations with the so-called ''chain-model.''[36] Here, the impact parameters are chosen aligned with the rows of the surface atoms; essentially two-dimensional calculations are performed on a three-dimensional (3D) crystal since the scattering is restricted to the plane given by the surface normal and the incoming angle. The calculations were done at $T=0$ and $T=300$ K, in order to study the influence of the thermal motion of the crystal atoms. To assure that only in-plane scattering occurs in the chain calculations at $T=300$ K, the crystal atoms are only displaced in the scattering plane. Enhanced vibrational amplitudes of the topmost surface layer have not been taken into account in the calculations because the study of this effect will take too much computational time, especially in the 3D calculations.

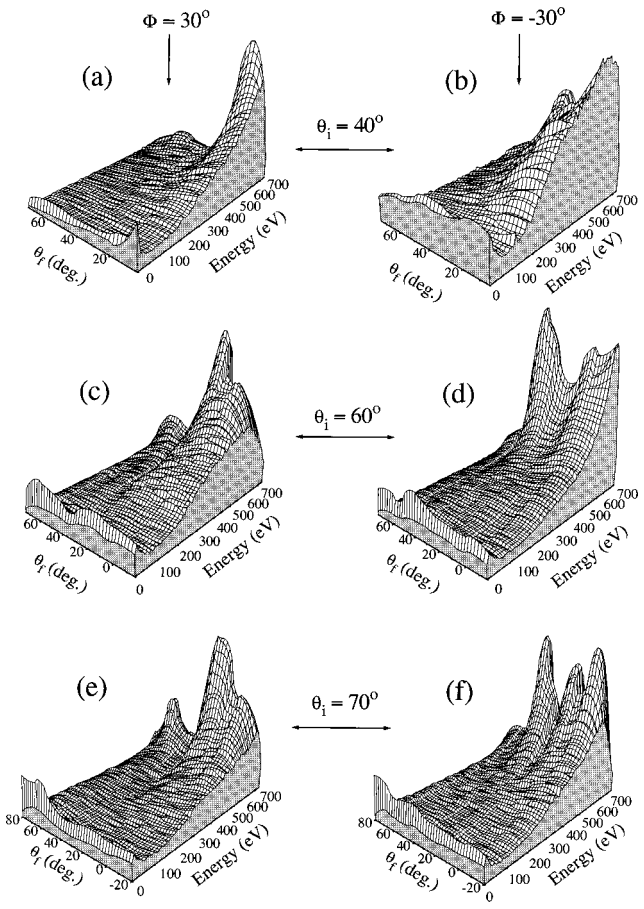

FIG. 2. Three-dimensional intensity distributions $I(\theta_f, E_f)$ for 700 eV H^+ from clean Ag(111) along the (112) or $\phi = 30°$ (a,c,e) and (211) or $\phi = -30°$ (b,d,f) azimuths for $\theta_i = 40°$ (a,b), $\theta_i = 60°$ (c,d) and $\theta_i = 70°$ (e,f). The measured intensities are plotted on a linear scale. Negatively charged hydrogen ions are detected. No correction for the energy-dependent transmission of the energy analyzer has been made.

IV. RESULTS AND ANALYSIS

A. Experimental results

1. *Scattering of* H^+ *from clean Ag(111)*

Figure 2 shows the energy and angular distributions of backscattered negative ions for 700 eV H^+ scattering off clean Ag(111) along the (112) (a,c,e) and (211) (b,d,f) azimuthal directions. These azimuthal directions are defined as $\phi = -30°$ and $\phi = 30°$, respectively. Spectra for three different incoming angles are plotted: $\theta_i = 40°$ (a,b), $\theta_i = 60°$ (c,d), and $\theta_i = 70°$ (e,f). Figure 2(a) shows scattering along the (112) or $\phi = 30°$ direction for an incoming angle of 40°. Two peaks can be observed at $\theta_f = 18°$ and $\theta_f = 58°$. These peaks are found at an energy position that corresponds to elastic scattering from a single Ag atom. Consequently, a binary collision model between an H ($M = 1$) and an Ag ($M = 109$) atom can be applied to explain the energy losses at the peak positions in the energy distributions. Figure 2(b) shows scattering along the (211) or $\phi = 30°$ direction. The incoming angle and energy are the same as in Fig. 2(a), but the energy distributions appear much broader and also the peak structures in the angular domain have changed. The energy losses the particles have suffered can be as large as 500 eV. However, the maximum energy loss in a binary collision between an H atom and an Ag atom is smaller than about 0.037 times the initial energy E_i, which suggests that the particles have traveled through many atomic layers before exiting the solid. Probably, a combination of elastic energy losses and electronic stopping is responsible for the observed energy losses. In Figs. 2(c) and 2(d) the incoming angle has been changed to 60°. The azimuthal orientations are identical to those in Figs. 2(a) and 2(b), respectively. The energy distributions for $\theta_i = 60°$ (c) have broadened compared to $\theta_i = 40°$ (a). Spectra (d) show a narrowing compared to spectra (b). Most likely, particles penetrate deeply into the crystal for certain combinations of θ_i and ϕ. Figures 2(e) and 2(f) show scattering for $\theta_i = 70°$. Now, the energy distributions have comparable widths. These particular scattering geometries do not give a penetration like that observed in Figs. 2(b) and 2(c). The peak positions in the outgoing angle seem to be independent of the incoming angle, which is an indication that these are due to the crystal structure. Similar peak structures have been observed for other systems.[37,38,29] The negative ions are primarily observed at small outgoing angles; at very grazing outgoing angles no negative ions are observed. This difference can be explained with the normal and parallel velocity effect in negative ion formation.[3]

To examine in more detail the peak structures in the outgoing angle we performed angular scans at one fixed final energy. Figure 3 shows angular distributions of H^- for 750 eV H^+ from clean Ag(111). The negative ions with a final energy of 708 eV are detected. Results for four different angles are shown, $\theta_i = 40°$ (a,e), $\theta_i = 60°$ (b,f), $\theta_i = 70°$ (c,g), and $\theta_i = 80°$ (d,h). Scattering occurs along the (112) or $\phi = 30°$ (a–d) and (211) or $\phi = -30°$ (e–h) azimuthal directions. For $\theta_i = 40°$ and $\phi = 30°$ [Fig. 3(a)], we clearly observe the two peaks at $\theta_f = 18°$ and $\theta_f = 58°$, which were present in Fig. 2(a). The absence of the scattering signal around $\theta_f = 35°$ is attributed to blocking of H atoms scattered from the second layer by atoms of the first layer. When we change the incoming angle to more grazing angles of incidence (b–d), we observe also a peak at $\theta_f = -5°$. This peak could not be observed for smaller angles of incidence because of the limited angular range of the detector. The peak positions are independent of the incoming angle, indicating that they are due to the exiting part of the trajectories the particles follow. At very grazing angles of incidence [$\theta_i = 80°$, Fig. 3(d)], we observe the appearance of two closely spaced peaks around $\theta_f = 76°$. This can be attributed to a surface rainbow, giving these two closely spaced peaks in the forward direction. It is remarkable that even for such grazing angles of incidence, penetration into the crystal lattice is observed.

Figures 3(e)–3(h) show scattering along the $(\overline{211})$ or $\phi = -30°$ azimuth. Three distinct peaks can be observed, around $\theta_f = -10°$, 10°, and 42°. Once again, the positions of the peaks are independent of the incoming angle. For $\theta_i = 80°$ two closely spaced peaks are again observed around $\theta_f = 76°$. These can be attributed to a surface rainbow.[21] Scattering along the (101) azimuth or $\phi = 0°$ also gives rise to peaks in the angular distributions, data which was previously published in Ref. 31.

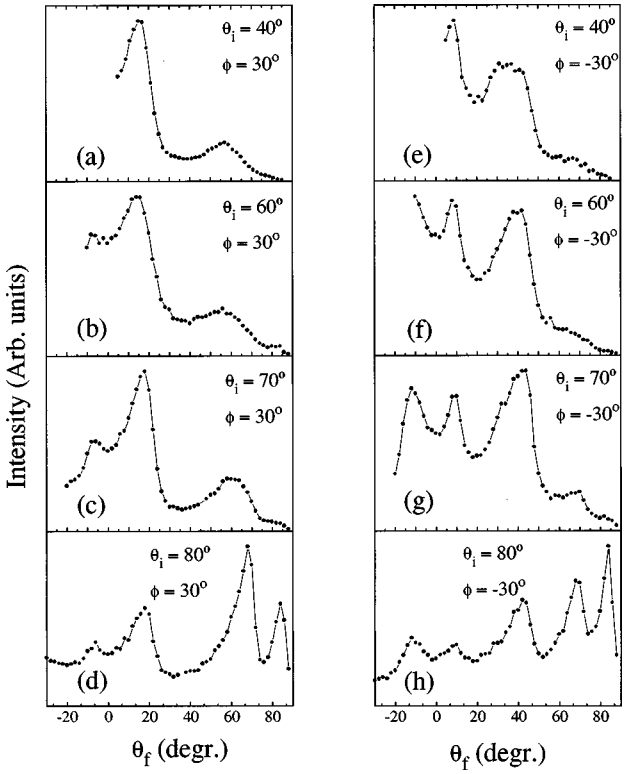

FIG. 3. Angular distributions of H^- for 750 eV H^+ from clean Ag(111). The negative ions with an energy of 708 eV are detected. Results for four different angles are shown: $\theta_i=40°$ (a,e), $\theta_i=60°$ (b,f), $\theta_i=70°$ (c,g), and $\theta_i=80°$ (d,h). Scattering occurs along the (112) or $\phi=30°$ (a–d) and (211) or $\phi=-30°$ (e–h) azimuthal direction.

To check whether the peak structures in the angular distributions are only due to the structure of the crystal, we also measured the angular distributions of the backscattered neutral hydrogen atoms, which are shown in Fig. 4. The incoming energy of the hydrogen ions is 750 eV and $\theta_i=70°$, scattering takes place along the (211) or $\phi=-30°$ azimuth; the same scattering conditions as employed in Fig. 3(g) for backscattered negative ions. The total yield of the backscattered neutral particles is measured with the fraction detector; the energy integrated angular distribution is measured. The angular distribution is strongly peaked around $\theta_f=82°$, a peak that was hardly visible in the negative ion case and can

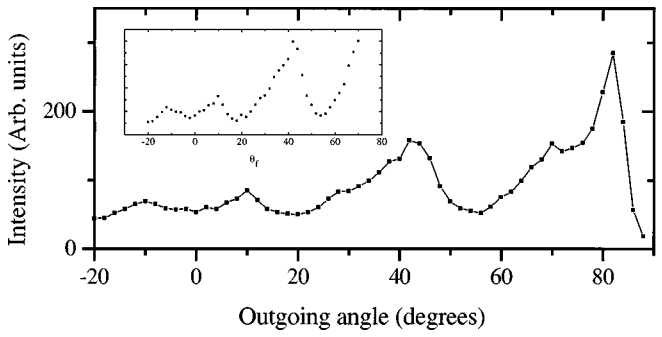

FIG. 4. Energy-integrated angular distribution of H atoms for 750 eV H^+ from clean Ag(111) along the (211) or $\phi=-30°$ azimuth. Data are taken at $\theta_i=70°$. The inset shows the same data but scaled differently, between $\theta_f=-20°$ and $\theta_f=70°$.

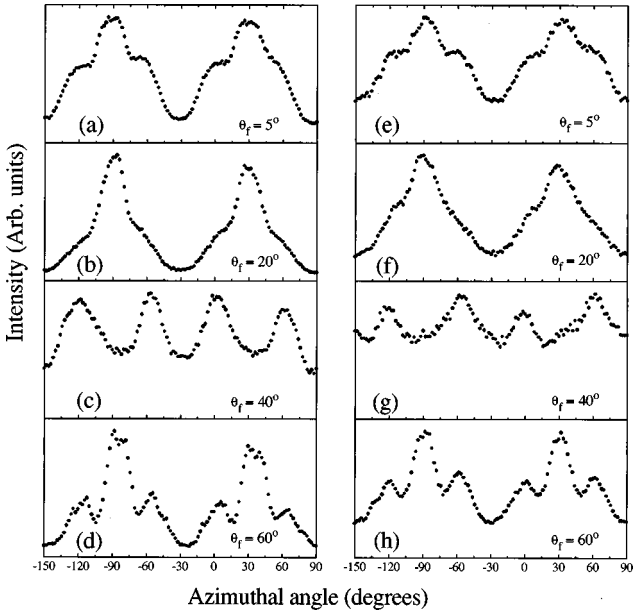

FIG. 5. Azimuthal dependence of backscattered H^- ions in scattering of H^+ from clean Ag(111) (left) and one monolayer of barium covered Ag(111) (right) for $\theta_i=40°$. The data are taken at $E_i=750$ eV and ions with a final energy of 708 eV (left) and 672 eV (right) are detected.

be attributed to surface rainbow scattering.[21] The peak structures between $\theta_f=-20°$ and $\theta_f=60°$ are the same as for the backscattered negative ions. The peaks are located at the same positions and also the relative peak heights are similar.

Another method to investigate the penetration into the crystal lattice is to perform azimuthal scans. Figure 5 (left panel) shows the azimuthal dependence of the backscattered H^- ions for 750 eV H^+ incident at clean Ag(111) and $\theta_i=40°$. The ions with a final energy of 708 eV are detected. Scans are performed at four different outgoing angles: (a) $\theta_f=5°$, (b) $\theta_f=20°$, (c) $\theta_f=40°$, and (d) $\theta_f=60°$, respectively. The spectra show a 120° symmetry, which indicates that more than one layer is involved in the scattering process. For $\phi=-30°\pm120°$ clear minima are observed in the spectra. This is because the first layer shadows the second layer and subsequent deeper layers, which allows for substantial penetration into the crystal lattice. The azimuthal scans reveal that the $\phi=0°,\pm60°,\ldots$ directions contribute equally to the backscattered signal. For these directions, the particles are focused into the surface channels and can be reflected by the second layer. The peaks that change significantly in intensity with outgoing angle are located at $\phi=-90°,30°,\ldots$. For these directions, at $\theta_f=5°$ and $\theta_f=20°$, the particles are scattered directly from the second layer and for $\theta_f=40°$, the particles reflecting from the second layer are blocked by the first layer. For $\theta_f=60°$ the particles show an increased yield because of the focusing effect; the particles can escape from the solid.

As a final point, in H^+ scattering off Ag(111) the relative yield of backscattered positive ions is very low ($<10^{-6}$) and they are hard to detect. In the case of $H_2{}^0$ and $H_2{}^+$ scattering from Ag(111), only first layer scattering was observed; the azimuthal scans showed a clear 60° symmetry of the backscattered H^+ ions, which were formed in a reionization process.[39]

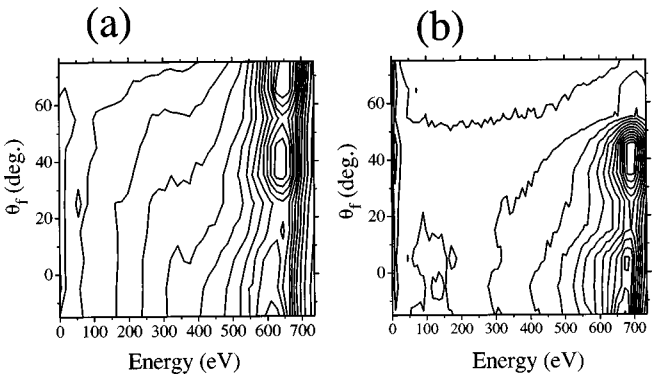

FIG. 6. Contour diagrams of backscattered negative ions for (a) 700 eV H^+ from one monolayer of barium-covered Ag(111) at $\theta_i = 60°$ along the (211) or $\phi = -30°$ azimuth and (b) for scattering of H^+ on clean Ag(111) for the same scattering geometry and incident energy. No correction for the energy-dependent transmission of the energy analyzer has been made.

2. *Scattering of* H^+ *from Ba/Ag(111)*

Covering the surface with barium and, hence, lowering the work function of the surface leads to an increase in negative ion yield.[3,29] Figure 6(a) shows the contour plot for H^- for 700 eV H^+ incident on Ag(111) covered by one monolayer of barium along the (211) or $\phi = -30°$ azimuth. The data are taken at $\theta_i = 60°$. The contour plot for scattering of H^+ on clean Ag(111) is also shown in Fig. 6(b) for the same scattering geometry and incident energy. This contour plot corresponds to the energy and angular distribution depicted in Fig. 2(d). The peaks in the angular distributions are located at the same positions as for the clean Ag(111) case, which indicates that the barium atoms are positioned at lattice position sites of the crystal. However, there are some remarkable differences for the two surfaces: (i) the energy distributions for scattering of Ba/Ag(111) are significantly broader than those measured from Ag(111), (ii) the peak positions of the energy distributions are shifted to lower energies by about 40 eV, for scattering of Ba/Ag(111), (iii) at grazing exit angles ($\theta_f > 50°$), a relative increase in negative ion yield is observed, and (iv) the yield of negative ions has increased from $<1\%$ for clean Ag(111) to around 20% for Ba/Ag(111).

To examine in more detail the effect of a barium overlayer on the negative ion signal, we display in Fig. 7 the energy distributions for two different outgoing angles, $\theta_f = 35°$ and $\theta_f = -15°$; these are cuts through the three-dimensional intensity distributions presented in Fig. 6. In Fig. 7(a) the energy distributions for scattering from Ag(111) are shown. For larger scattering angles the measured peak energy position shifts to lower energies; more energy is transferred to the surface. These peak positions agree with the peak positions calculated from the binary collision formula, with $M_H = 1$ and $M_{Ag} = 109$.[1,5,2] Figure 7(b) shows the energy distributions for scattering from Ba/Ag(111). Clearly, the peak positions are observed at lower energies than in Fig. 7(a). The elastic scattering positions, as calculated from the binary collision formula, are indicated with arrows; the particles have suffered an additional energy loss of 50 eV. For larger scattering angles, the peak positions shift to lower energies. In addition, a considerable broadening of the peaks is

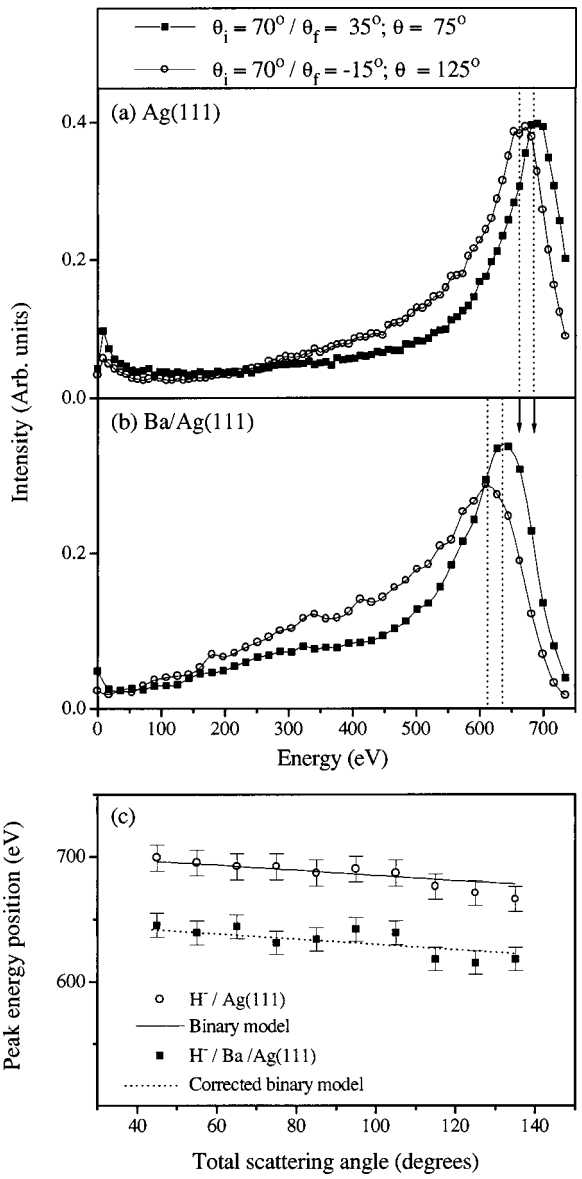

FIG. 7. Intensity distributions of backscattered negative ions for 700 eV H^+ at $\theta_i = 70°$ on (a) clean Ag(111) and (b) on one monolayer of barium-covered Ag(111) surface. (c) shows the peak energy positions as a function of total scattering angle θ for scattering of these surfaces. The lines in (c) were calculated from the binary collision model for the H on Ag system (solid line) and corrected for H on Ba/Ag (dashed line).

observed. For $\theta_f = 35°$, the width (full width at half maximum) is about 120 eV in the case of the clean Ag(111) and 145 eV in the case of scattering from the Ba/Ag(111) surface. In Fig. 7(c) the peak positions in the energy distributions are depicted for scattering from Ag(111) and Ba/Ag(111) as a function of total scattering angle. The solid line gives the calculated energy position as extracted from the binary collision formula; clearly, the data points are described fairly well by this model calculation. The measured energy losses from the Ba/Ag(111) surface are much larger than are to be expected on the basis of the binary collision formula. The dashed line gives the energy positions for elastic scattering displaced to lower energies by about 50 eV, to obtain a fit with the data points. The energy losses with outgoing angle are reproduced by the binary collision model.

However, the 50 eV additional energy loss is due to inelastic effects.

Figure 5 (right) shows the azimuthal dependence of the H^- yield for 750 eV H^+ incident at one monolayer of barium-covered Ag(111). The ions with final energies of 672 eV are detected. The scans appear identical to the spectra taken for clean Ag(111) (left), except the background signal seems to be higher. The results of the angular and azimuthal scans appear to clearly indicate that the barium atoms are located at lattice positions of the Ag(111) substrate.

Until now, we have attributed the observed structure in the azimuthal scans to particles following different kinds of trajectories in the solid/surface region. We did not take crystallographic effects in neutralization or negative ion formation probabilities into account. A way to check the validity of this assumption is performing an azimuthal scan with the fraction detector and determining the fraction of negative ions as a function of the azimuthal orientation of the crystal. This approach was previously applied by Närmann and coworkers in their study on crystallographic effects in charge exchange processes.[27] They studied He^+ from Ni(110) at grazing angles of incidence, and found minima in the charge fraction $He^+/(He^0+He^+)$ along the major crystallographic directions. This effect was attributed to different trajectories and different contributions of Auger neutralization and ''dynamic resonant loss processes.'' Also van Slooten followed this procedure in Ref. 40.

Figure 8 shows the azimuthal dependence of backscattered (a) H^0 and (b) H^- particles in scattering of H^+ from two layers of barium-covered Ag(111) for $\theta_i=40°$ and $\theta_f=40°$. The data are taken at $E_i=1250$ eV and the energy integrated signals are measured with the fraction detector. The signals for neutral atoms and negative ions show identical behavior. The fraction $I(H^-)/[I(H^-)+I(H^0)]$ shows no variation with azimuthal angle as can be seen in Fig. 8(c); its value is constant at 0.22, in agreement with a previous study.[29] We do not observe crystallographic effects in negative ion formation within the experimental error and therefore we conclude that observed structures in the azimuthal scans are due to scattering effects.

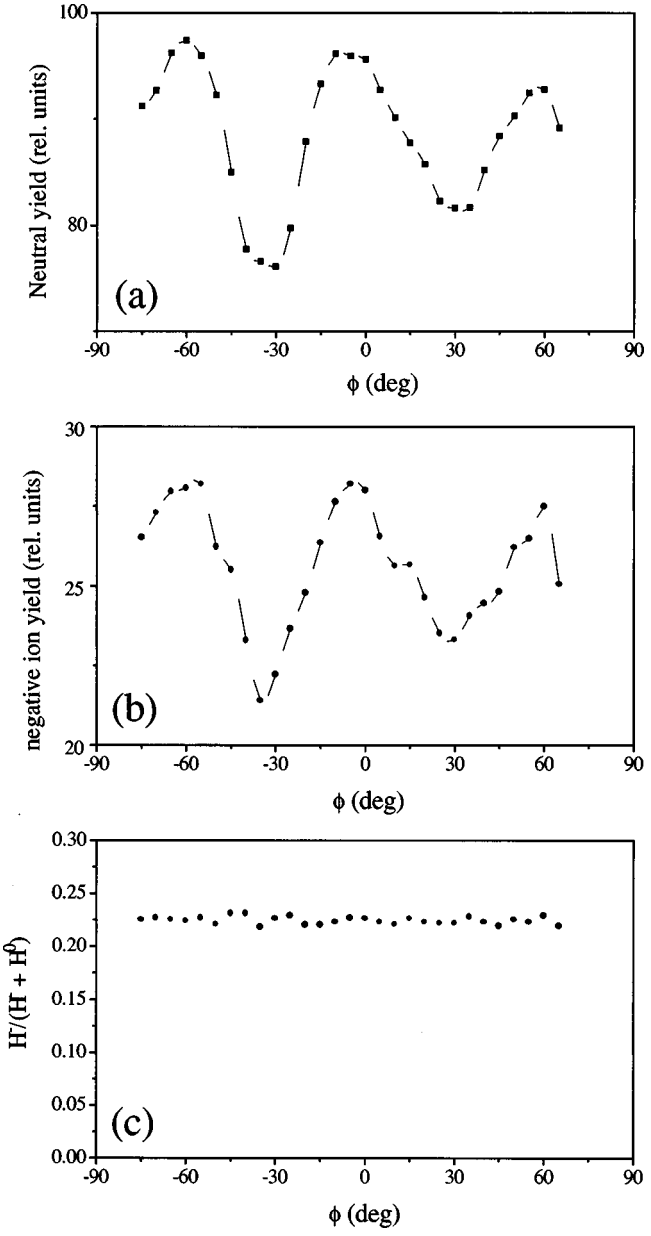

FIG. 8. Azimuthal dependence of backscattered (a) H^0 and (b) H^- particles in scattering of H^+ from two layers of barium-covered Ag(111) for $\theta_i=40°$ and $\theta_f=40°$. The data are taken at $E_i=1250$ eV and the energy integrated signals are measured. Also shown in (c) is the fraction of negative ions.

B. Classical trajectory calculations

To assign the peaks in the angular distributions to classes of trajectories, we performed classical trajectory calculations. Figure 9(a) displays the calculated angular spectra for 750 eV H scattering from the Ag(111) surface with impact parameters aligned along the (211) or $\phi=-30°$ azimuth. The crystal temperature is set at 0 K, $\theta_i=70°$, and 20 000 trajectories are calculated. The calculated spectra show the same peak structures as were observed for experimental angular distributions, although in this case the peaks are much narrower. The positions of the peaks in the calculations agree fairly well with those observed in the experimental results. The calculated peaks are located at $\theta_f=-10°$, 10°, 44°, 70°, and 82°, respectively. In the chain calculation only trajectories are considered that scatter in the plane given by the surface normal and the incoming angle. This is only a small fraction of the scattering events that take place; when the impact parameters are not chosen exactly on top of the crystal row, extensive out-of-plane scattering occurs.[41,36]

At the backscattering directions two additional peaks are observed at $\theta_f=-78°$ and $\theta_f=-56°$; these were not observed in the experiment because of the limited range of the detector position. The peak at $\theta_f=-78°$ is due to to a backward rainbow in an analysis of the trajectories.[42] The rainbow position is shifted towards the surface normal by about 4° compared to the rainbow in the forward scattering direction. In the forward scattering direction relatively soft collisions lead to rainbow scattering, and in backward scattering hard collisions are important. The peak at $\theta_f=-56°$ is observed in scattering along the (112) or $\phi=30°$ axis. This direction is the same as the (211) or $\phi=-30°$ direction rotated over 180°. The peak was due to particles directly scattered from the second layer; particles at smaller outgoing angles are ''blocked'' by the first layer.[42]

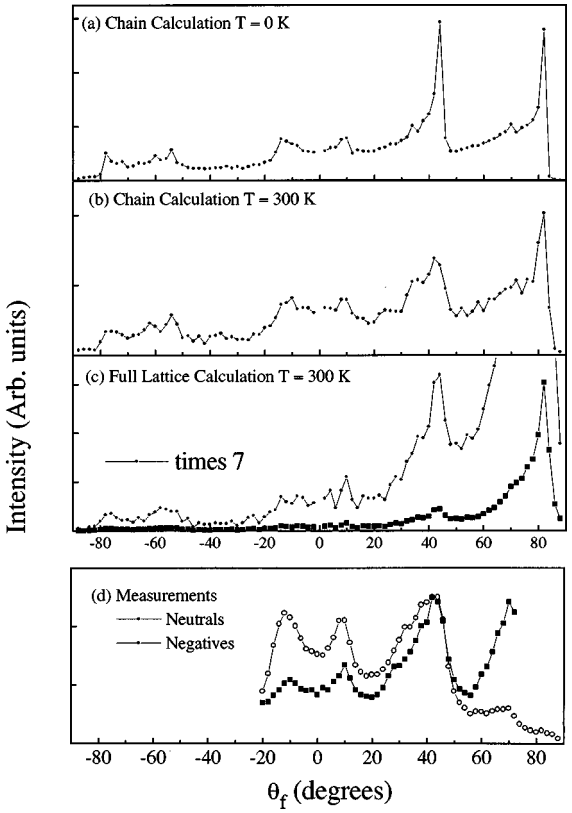

FIG. 9. Calculated angular spectra for 750 eV H scattering from the Ag(111) surface along the (211) or $\phi=-30°$ azimuth, for $\theta_i=70°$. (a) ''Chain'' calculation for $T=0$ K. (b) ''Chain'' calculation for $T=300$ K. (c) 3D calculation for $T=300$ K. In (d) the measurements for scattered neutrals and negatives are displayed.

In Fig. 9(b) the thermal vibrations of the crystal atoms are included ($T=300$ K). The average displacements of the crystal atoms is approximately 0.01 Å.[43] Once more, 20 000 trajectories are calculated with impact parameters centered over the top-layer atom chains. In the angular spectra a significant broadening of the peaks is observed compared to the $T=0$ K case, but the calculated peak positions are not affected. The rainbow is the dominant feature in the spectrum and its appearance remains sharp. The backscattered rainbow is also still observed. For systems where the range of the potential is of the same order as the internuclear distances between the surface atoms, the backward rainbow is very sensitive to surface temperature, and disappears at sufficiently high temperatures.[21,36,44] Our results show that a backscattered rainbow is still observed at $T=300$ K. In the H-Ag system the range of the potential is an order of magnitude smaller than the internuclear distance between the surface atoms.

In a 3D calculation at $T=300$ K, even better agreement with the experimental data is obtained. However, to get reasonable statistics, 50 times more trajectories (i.e., 1×10^6) are calculated than was required in the chain calculations. The calculation is shown in Fig. 9(c). The impact parameters are no longer chosen aligned with the rows of the surface atoms, but systematically on a grid over the entire surface unit cell. The peak positions, their widths, and the peak heights of the rainbow peak agree fairly well with the data [Fig. 9(d)]. The yield of particles at large backscattering angles is underestimated due to the limited size of the crystal in the calculation (321 atoms). The most striking difference between the chain calculation and the 3D calculation is the increase of the rainbow peak relative to the other peaks originating from deeper in the crystal; out-of-plane scattering becomes important and the effect increases for multiple collisions. It seems that the peaks for sufficiently small energy losses can be explained by in-plane scattering, especially considering the good agreement between the experimental data and the chain calculations.

In Fig. 10(a), the calculated trajectories for 750 eV H^0 with impact parameters along the (211) or $\phi=-30°$ axis of the Ag(111) surface are depicted. The beam is incident at (a) $\theta_i=70°$ and the crystal temperature is set at 0 K; the same scattering conditions as in Fig. 9(a). We can see that the particles can penetrate deep into the crystal and that they follow complicated zigzag trajectories through the crystal. Direct scattering from the third and fourth layers appears to be important.

A more direct way to check the origin of the peaks in the angular distributions is reversing the trajectories, i.e., changing the incoming angles of the beam to the outgoing angles where the peaks appear. This approach is valid because the energy losses the particles suffer at the peak positions are small. The peak maxima appear at the position for elastic scattering. We first look at the origin of the peaks located at $\theta_f=-10°$ and 10°. In Figs. 10(b)–10(d), beams of particles are incident at (b) $\theta_i=10°$, (c) 0°, and (d) $-10°$, respectively. For $\theta_i=-10°$ and $\theta_i=10°$ direct scattering from the second, third, fourth, and even fifth layers is observed. When a beam of particles is incident at 0° only direct scattering from the second and third layers is observed. The fourth layer is shadowed by the first and the fifth by the third. Now we can assign the two peaks in the angular spectra at $\theta_f=-10°$ and 10° to ''direct'' scattering from the fourth and fifth layers. At $\theta_f=0°$ a minimum is observed that can be attributed to blocking of the particles by the second and third layers. The same approach can be made for the peak at $\theta_f=44°$. Here, also direct scattering from the second, third and fourth layers is important. In the analysis the focusing effect is important. Next to a blocking minimum we find maxima in intensity due to the enhanced flux of particles at the edges of the shadow cones. The peak at $\theta_f=70°$ is identified with a crystal channel identical to the one observed in Fig. 10(a), where $\theta_i=70°$ and the particles penetrate along this direction.

V. DISCUSSION

A. Penetration depth and energy losses

1. *Scattering of* H^+ *from clean Ag(111)*

The experimental results and classical trajectory calculations reveal that the number of particles reflected from the solid is highly dependent on the crystal azimuth along which scattering occurs. Experimentally, this is demonstrated in the azimuthal scans; for $\theta_i=40°$, approximately five times more backscattering occurs along the (112) or $\phi=30°$ direction than along the (211) or $\phi=-30°$ direction (see Fig. 5). In the classical trajectory calculations, the ratio of 5:1 is reproduced (not shown).[42] The calculations indicate that for scat-

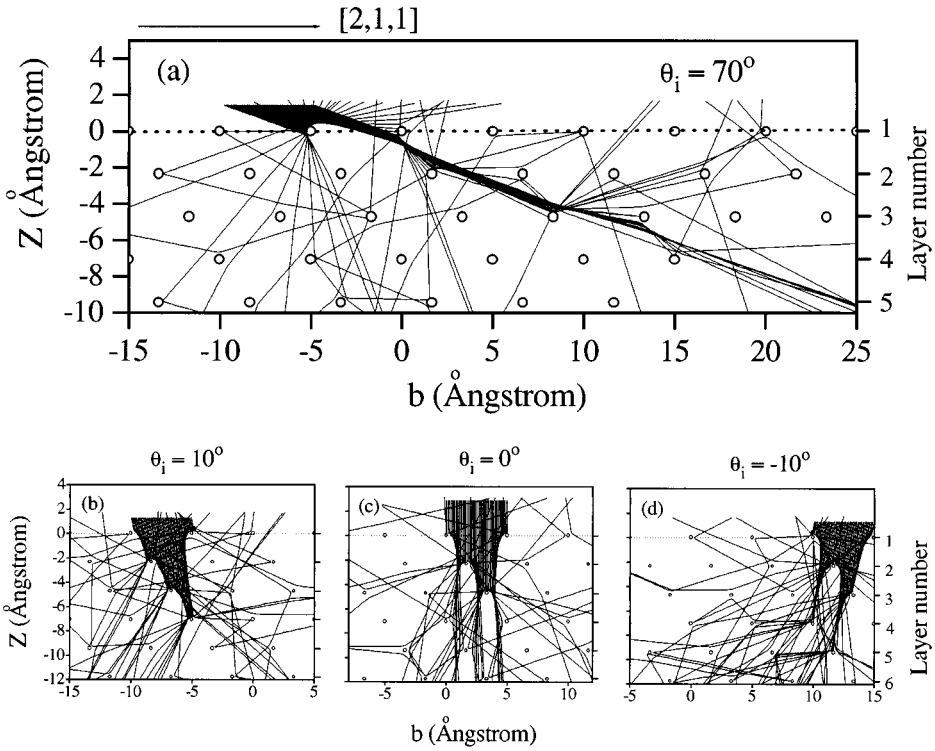

FIG. 10. Calculated trajectories for 750 eV H^0 with impact parameters along the $(2\bar{1}1)$ or $\phi = -30°$ axis of the Ag(111) surface. The beams are incident at (a) $\theta_i = 70°$, (b) $\theta_i = 10°$, (c) $\theta_i = 0°$, and (d) $\theta_i = -10°$.

tering along the $(11\bar{2})$ or $\phi = 30°$ direction, about 25% of the *total* incident H particles are backscattered. However, this is a chain calculation and many particles can penetrate between the crystal rows. In the case of 3D calculations and scattering along the (211) or $\phi = -30°$ azimuth and $\theta_i = 70°$, the total reflection is about 20% and, consequently, 80% is implanted in the crystal lattice. However, the total amount of particles that is reflected in the experiment may be higher, because in the classical trajectory calculations we only consider a crystal lattice consisting of five layers; reflection from deeper layers was not taken into account.

In what follows, we make an estimate of the distances the particles have traveled inside the solid. With the help of Fig. 10 we have made an analysis of the trajectories the particles have followed that give rise to the observed peaks at $\theta_f = -10°$ and $\theta_f = -10°$ for $\theta_i = 70°$. These peaks were assigned to trajectories coming ''directly'' from the fourth and fifth layers. When we take the minimal distance the particles have traveled to reflect from the fourth and fifth layers, these lengths are 35 and 45 Å, respectively. The extrapolated value for the stopping power of hydrogen in a Ag solid is given by 2.8 eV/Å, at translational energies of 700 eV.[45] This value is close to the value used by Van Wunnik *et al.* in H^+ scattering from a tungsten surface, i.e., 3.0 eV/Å.[46] Note that these are extrapolated values, below 10 keV no experimental stopping power data are shown in Ref. 45; a square-root dependence with energy is assumed in the extrapolation procedure. When the particles have traveled 35 Å, an energy loss of about 100 eV is expected. However, particles originating from the fourth layer are observed at a peak energy position, which can be explained solely on the basis of the binary collision model (see Fig. 7). From this we estimate that the (electronic) stopping power must be at least one or two orders of magnitude smaller than that extrapolated by Andersen and Ziegler,[45] i.e., <0.3 eV/Å. When we assume a constant stopping power between energies of 700 and 200 eV, the particles that have suffered energy losses of 500 eV must have traveled over a distance larger than 1700 Å. Particles that have experienced even larger energy losses must have traveled over distances on the order of μm s.

2. Scattering of H^+ from Ba/Ag(111)

Some distinct differences in the H^- energy distributions are observed when scattering H^+ from a clean and from one monolayer of barium covered Ag(111) surface. For the barium case, the energy distributions appear broader and for incoming energies of 700 eV, the peak positions are lowered by about 50 eV relative to those of scattering from a clean Ag(111) surface, for identical scattering conditions (Fig. 7). Moreover, scattering off two monolayers of barium leads to the same additional 50 eV energy loss,[29] which indicates that these losses are not due to bulk properties of the barium. The tabulated value for the electronic stopping in bulk Ba is 1.0 eV/Å at energies of $E = 700$ eV, 2.8 times smaller than the value in bulk Ag.[45] However, Andersen and Ziegler do not show any experimental data for the Ba case; the stopping powers are solely based on calculations.

The peak structures in the angular distributions are identical for scattering from a clean Ag(111) surface and from a Ag(111) surface covered with one monolayer of barium (see Fig. 6). The hydrogen particles must have followed identical trajectories for both surfaces, therefore the higher-energy losses cannot be explained by different trajectories and, hence, different elastic energy losses. Clearly, the additional energy losses must be related to a surface effect; either the

lowering of the work function and/or the increase in electron density near the Fermi level. The work function of a clean Ag(111) surface is 4.7 eV, while that of Ba/Ag(111) is 2.4 eV. In the case of scattering from a graphite surface (work function of 5 eV), an appreciable negative ion yield (about 20%) is measured, but the H^- are observed at the elastic scattering position of a H-C collision.[7] Also for scattering from Pt(111), with a work function of 5 eV, the energy losses can be explained by the binary collision formula.[7] However, in the case of H^+ scattering from Cs/W(110) (work function of 1.9 eV) the observed energy losses of the H^- are larger than expected on the basis of the binary collision model, between 5% and 15% instead of 0.5% as calculated by the binary collision model.[46] These observations suggest that scattering off a low work-function surface leads to additional energy losses that cannot be explained by the binary collision formula.

Higher-energy losses for the H^- have also been observed in scattering H^+ from potassium-covered Pd(110), compared to scattering off clean Pd(110) by Höfner, Närmann, and Heiland.[47] They attributed this to the lowering of the work function, which is associated with an increased electron charge density at the surface, giving rise to higher stopping powers. The effective interaction region is enhanced, leading to larger energy losses. These experiments were carried out for grazing angles of incidence. In our case, the particles do not spend most of their time in the surface region, but deeply penetrate into the crystal lattice.

Possibly, electron capture and loss processes during the particle/surface interaction are responsible for the higher-energy losses in the case of scattering off a low work-function surface as suggested in Ref. 47. In bulk material, dynamic loss and capture processes are supposed to contribute to the observed energy losses.[48] In ion/surface collision these occur, for low work-function surfaces, on the incoming and outgoing trajectory. The times spent in the ion/surface interaction region are distinctly different for high and low work function surfaces, considering the shift of the affinity level due to the image force and the location of the Fermi level. Recent experimental results of light ions scattered off Al(110) and K/Pd(110) indicate that calculated bulk friction coefficients cannot be used to explain the observed energy losses and that the friction of light ion is different at the surface and in the bulk.[49]

The width of the hydrogen affinity level is at most 1.3 eV between 0.4 and 1.25 Å from the surface image plane, in the case of one monolayer of barium-covered surface.[29] Applying Heisenberg's uncertainty relationship, we obtain a typical transition rate w of 2×10^{14} s^{-1}. The velocity of an hydrogen particle of $E=700$ eV is $v=3.7\times10^{15}$ Å s^{-1}. For particles leaving low work-function surfaces, the affinity level will be resonant with the conduction band longer, allowing for more transitions and hence more friction, than for particles leaving a high work-function surface, at the same $v_\perp$. However, more experiments and analysis are necessary to verify this conclusion.

B. Surface structure analysis: Location of the barium atoms

The azimuthal scans and angular distributions of H^- scattered from clean Ag(111) and one monolayer of barium-covered Ag(111) appear identical. Only the yield of negative ions as a function of outgoing angle is different, which we attribute to different angular dependencies of negative ion formation. The scattering data, together with the classical trajectory calculations strongly suggest that the barium atoms occupy threefold hollow sites of the Ag(111) lattice. The classical trajectory calculations indicate that if the barium atoms are located at positions other than the fcc threefold hollow sites, the angular distributions would look dramatically different. Previous studies on the adsorption of barium on Ag(111) suggest the formation of a complete monolayer with a density of 0.61×10^{15} particles/cm^2, after which a rather open overlayer is formed by Poisson growth.[14] The results in the current paper indicate that threefold hollow (fcc) sites are occupied. The density of the barium overlayer is lower than that of the Ag substrate layer as was indicated by previously obtained MEIS results.[14] This was attributed to the larger size of the barium atoms. However, we cannot give the long-range order of the barium overlayer because we are not sensitive to that. Epitaxial growth with vacancies to accommodate the large adsorbate atoms has also been found by Lamble and King.[50] They studied the adsorption of Cs on Ag(111) with extended x-ray-absorption fine structure and found a very open structure with all the Cs atoms sitting at the threefold hollow sites. Perhaps a structural study using another structure sensitive technique will shed more light on the long-range order of the barium overlayer.

Using the detection of backscattered negative hydrogen ions in ion beam crystallography studies with low-energy protons incident on metal surfaces, appreciable depth information can be obtained. In this paper we have demonstrated that we can distinguish ions coming from the second layer and ions coming from the fourth and even the fifth layers. With the detection of backscattered positive ions this is not possible in the low incident energy regime, because of extensive neutralization of the ions when penetration into the solid occurs. This depth information can be achieved in LEIS, when backscattered neutrals are detected. However, in the case of negative ions (H^-) an electrostatic analyzer can be used and, hence, energy analysis on the backscattered ions can be performed; elemental specific information can be obtained. Especially in conjunction with ''conventional'' LEIS using He^+ or Ne^+, the detection of negatively charged hydrogen ions gives additional information concerning the structures of overlayers deposited onto metal surfaces.

VI. SUMMARY AND CONCLUSIONS

In the scattering of H^+ from a clean and one monolayer of barium-covered Ag(111) surface, reflection from deeper layers is observed. The backscattered negative and neutral hydrogen particles show the same angular and azimuthal dependencies. The differences in the angular behavior are explained with a difference in negative ion formation as a function of outgoing angle. The final charge state of the particles is determined on exiting the surface layer. The energy distributions of the negative ions indicate a large penetration depth along the crystal channels. Classical trajectory calculations reproduce the qualitative features of the angular distributions of the neutral and negative particles and an assignment of the trajectories has been made. The extrapolated

HFS/LCAO (linear combination of atomic orbitals) Ag-H pair potential used in these calculations describes the interaction very well. For the scattering conditions used in this study, the interaction between the H atom and Ag atoms can be considered a sequence of binary collisions. The (electronic) stopping inside the Ag solid is at least one or two orders of magnitude smaller (<0.3 eV/Å at $E=700$ eV) than the values found in literature.

The energy losses of the detected H^- in scattering from a clean Ag(111) surface are accounted for by the binary collision formula. In scattering from a Ba/Ag(111) surface, additional inelastic energy losses of the scattered ions are observed, which are due to the lowering of the work function and/or an increase of the electron density near the Fermi level. The negative ion fraction in the Ag case decreases at smaller outgoing angles than in the Ba/Ag case. The high work function of the Ag(111) surface allows for more time for the negative ion to donate back its electron for a similar $v_\perp$. No trajectory-dependent charge-transfer events have been observed in scattering from a Ba/Ag(111) surface.

The angular distributions and azimuthal scans do not significantly change with covering the Ag(111) surface with one monolayer of barium. This indicates that the barium atoms must sit in the threefold hollow (fcc) sites of the surface. The layer must contain vacancies to accommodate the large barium atoms on the substrate. Appreciable depth information can be obtained in surface structure analysis studies via the detection of negatively charged low-energy hydrogen ions.

ACKNOWLEDGMENTS

The authors would like to thank F. G. Giskes and R. Schaafsma for technical support, and T. L. Weeding and M. Gleeson for carefully reading the manuscript. We acknowledge the European Science Foundation (program on Dynamics of Gas-Surface Interactions) (D.V.) for financial support. This work is part of the research program of the Foundation of Fundamental Research on Matter (F.O.M.) with the financial support (in part) of The Netherlands Technology Foundation (S.T.W).

*On leave from Department of Physics, University of Ioannina, Gr-451 10 Ioannina, Greece.

†Present address: Philips Natuurkundig Laboratorium, Prof. Holstlaan, 5656 AA Eindhoven, The Netherlands.

‡FAX: X-31-20-6684106. Electronic address: kleyn@amolf.nl

[1] S. R. Kasi, H. Kang, C. S. Sass, and J. W. Rabalais, Surf. Sci. Rep. **10**, 1 (1989), and references therein.

[2] H. Niehus, W. Heiland, and E. Taglauer, Surf. Sci. Rep. **17**, 213 (1993), and references therein.

[3] J. Los and J. J. C. Geerlings, Phys. Rep. **190**, 133 (1990), and references therein.

[4] B. H. Cooper and E. R. Behringer, in *Low Energy Ion-Surface Interactions*, edited by J. W. Rabalais (Wiley, Chichester, UK, 1994).

[5] P. G. Betrand and J. W. Rabalais, in *Low Energy Ion-Surface Interactions*, edited by J. W. Rabalais (Wiley, Chichester, UK, 1994).

[6] C. F. A. Van Os, P. W. Van Amersfoort, and J. Los, J. Appl. Phys. **64**, 3863 (1988).

[7] K. Tsumori, W. R. Koppers, R. M. A. Heeren, M. F. Kadodwala, J. H. M. Beijersbergen, and A. W. Kleyn, J. Appl. Phys. **81**, 6390 (1997).

[8] M. Hou and M. T. Robinson, Appl. Phys. **17**, 295 (1978).

[9] D. P. Jackson and W. Eckstein, Nucl. Instrum. Methods Phys. Res. **194**, 671 (1982).

[10] W. Eckstein and J. P. Biersack, Appl. Phys. A: Solids Surf. **38**, 123 (1985).

[11] R. Aratari and W. Eckstein, Nucl. Instrum. Methods Phys. Res. B **42**, 11 (1989).

[12] M. Shi, J. W. Rabalais, and V. A. Esaulov, Radiat. Eff. Defects Solids **109**, 81 (1989).

[13] H. Muller, R. Hausmann, H. Brenten, and V. Kempter, Surf. Sci. **284**, 129 (1993).

[14] U. van Slooten, W. R. Koppers, H. M. van Pinxteren, A. M. C. Moutinho, J. W. M. Frenken, and A. W. Kleyn, J. Phys.: Condens. Matter **5**, 5411 (1993).

[15] C. Höfner, A. Närmann, and W. Heiland, Nucl. Instrum. Methods Phys. Res. B **72**, 227 (1992).

[16] R. J. MacDonald, D. J. O'Connor, B. V. King, Y. Shen, and G. Xu, Nucl. Instrum. Methods Phys. Res. B **78**, 56 (1993).

[17] B. V. King, D. J. O'Connor, and G. Xu, Radiat. Eff. Defects Solids **130**, 293 (1994).

[18] C. Auth, A. G. Borisov, and H. Winter, Phys. Rev. Lett. **75**, 2292 (1995).

[19] H. Winter, A. G. Auth, and A. G. Borisov, Nucl. Instrum. Methods Phys. Res. B **115**, 133 (1996).

[20] M. Maasouz, L. Guillemot, S. Lacombe, and V. A. Esaulov, Phys. Rev. Lett. **77**, 4265 (1996).

[21] A. W. Kleyn and T. C. M. Horn, Phys. Rep. **199**, 191 (1991).

[22] A. D. Tenner, K. T. Gillen, T. C. M. Horn, J. Los, and A. W. Kleyn, Surf. Sci. **172**, 90 (1986).

[23] A. D. Tenner, R. P. Saxon, K. T. Gillen, D. E. Harrison, Jr., T. C. M. Horn, and A. W. Kleyn, Surf. Sci. **172**, 121 (1986).

[24] C. A. Keller, C. A. DiRubio, G. A. Kimmel, and B. H. Cooper, Phys. Rev. Lett. **75**, 1654 (1995).

[25] G. E. Makhmetov, A. G. Borisov, D. Teillet-Billy, and J. P. Gauyacq, Surf. Sci. **366**, L769 (1996).

[26] F. Wyputta, R. Zimny, and H. Winter, Nucl. Instrum. Methods Phys. Res. B **58**, 379 (1991).

[27] A. Närmann, H. Derks, W. Heiland, R. Monreal, E. Goldberg, and F. Flores, Surf. Sci. **217**, 255 (1989).

[28] D. J. O'Connor, R. J. MacDonald, W. Eckstein, and P. R. Higginbottom, Nucl. Instrum. Methods Phys. Res. B **13**, 235 (1986).

[29] U. van Slooten, O. M. N. D. Teodoro, A. W. Kleyn, J. Los, D. Teillet-Billy, and J. P. Gauyacq, Chem. Phys. **179**, 227 (1994).

[30] D. Teillet-Billy and J. P. Gauyacq, Surf. Sci. **239**, 343 (1990).

[31] W. R. Koppers, B. Berenbak, D. Vlachos, U. van Slooten, and A. W. Kleyn, Nucl. Instrum. Methods Phys. Res. B **100**, 417 (1995).

[32] A. Bot, U. van Slooten, W. R. Koppers, and A. W. Kleyn, Surf. Sci. **287**, 901 (1993).

[33] E. J. J. Kirchner, E. J. Baerends, U. van Slooten, and A. W. Kleyn, J. Chem. Phys. **97**, 3821 (1992).

[34] U. van Slooten, E. J. J. Kirchner, and A. W. Kleyn, Surf. Sci. **283**, 27 (1993).

[35] M. T. Robinson and I. M. Torrens, Phys. Rev. B **9**, 5008 (1974).

[36] D. L. Adler and B. H. Cooper, Phys. Rev. B **43**, 3876 (1991).
[37] H. B. Nielsen and T. A. Delchar, Surf. Sci. **141**, 487 (1984).
[38] M. N. Yusuf and T. A. Delchar, Surf. Sci. **182**, 231 (1987).
[39] U. van Slooten, D. R. Anderson, A. W. Kleyn, and E. A. Gislason, Surf. Sci. **274**, 1 (1992).
[40] U. van Slooten, Ph.D. thesis, University of Amsterdam, 1993.
[41] R. L. McEachern, D. M. Goodstein, and B. H. Cooper, Phys. Rev. B **39**, 10 503 (1989).
[42] W. R. Koppers, Ph.D. thesis, University of Amsterdam, 1997.
[43] R. Lahaye, Ph.D. thesis, Vrije Universiteit Amsterdam, 1995.
[44] R. J. W. E. Lahaye, S. Stolte, S. Holloway, and A. W. Kleyn, Surf. Sci. **338**, 169 (1995).
[45] H. H. Andersen and J. F. Ziegler, *The Stopping and Ranges of Ions in Matter*, edited by J. F. Ziegler (Pergamon, New York, 1977), Vol. 1.
[46] J. N. M. van Wunnik, J. J. C. Geerlings, E. H. A. Granneman, and J. Los, Surf. Sci. **131**, 17 (1983).
[47] C. Höfner, A. Närmann, and W. Heiland, Nucl. Instrum. Methods Phys. Res. B **93**, 113 (1994).
[48] A. Närmann, W. Heiland, R. Monreal, F. Flores, and P. M. Echenique, Phys. Rev. B **44**, 2003 (1991).
[49] S. Hausman, C. Höfner, T. Schlathölter, H. Franke, A. Närmann, and W. Heiland, Nucl. Instrum. Methods Phys. Res. B **115**, 31 (1996).
[50] G. M. Lamble and D. A. King (private communication).